Insight into the Synergetic Effect in Ternary Gold-Based Catalysts: Ultrastability and High Activity of Au on Alumina Modified Titania

Chuan-Ming Wang, Kang-Nian Fan, and Zhi-Pan Liu*

Shanghai Key Laboratory of Molecular Catalysis and Innovative Materials, Department of Chemistry, Fudan University, Shanghai 200433, China

Received: June 12, 2007; In Final Form: July 14, 2007

Nanogold particles dispersed on oxides can be highly active as catalyst and often lack the long-term stability due to the inherent instability of small gold particles. New thinking for the catalyst design is therefore urgently demanded to enhance the gold sticking on oxides while retaining the high activity. By systematically investigating the working mechanism of a ternary system, Au supported on alumina modified anatase titania, using first principles calculations, this work illustrates from the atomic level how a third component (alumina) can be used as the nucleation center to anchor Au particles while the component itself does not take part in the catalytic oxidation of CO. For Au supported on pure anatase, CO oxidation is already facile with the reaction barrier being only 0.22 eV, but the Au adsorption on anatase is rather weak as expected. The stepwise growth of alumina on anatase is shown to produce locally clustered alumina thin layers on anatase (Al_2O_3/TiO_2). On these Al_2O_3/TiO_2 sites, the binding energy of Au can be more than five times that on pure anatase. The active site of CO oxidation in the ternary system, however, remains at the boundary of Au/anatase, since it is found that O_2 does not adsorb at the boundary between Au and Al_2O_3 thin films. Electronic structure analyses are utilized to rationalize the results. The synergetic effect revealed here implies that applying nonuniform mixed-oxide support could be a promising solution toward practical applications of Au-based catalysts.

1. Introduction

The activity and stability of the catalyst are two fundamental issues in catalysis.[1−5] A fine balance between them is the prerequisite for high catalytic performance. For the oxide-supported Au catalysts, a class of promising materials to catalyze a variety of important chemical reactions,[6−16] their activity usually drops sharply with respect to the operating time.[17−20] One of the key reasons for the catalyst deactivation is the agglomeration of Au particles.[20] Since the activity of most gold-based catalysts originates from the intimate contact boundary between small Au particles and oxide supports,[21−23] the population of which diminishes as small Au particles start to agglomerate under catalytic conditions, a challenging question in the field is thus how to retain the high activity of the thermodynamically unstable Au/oxide structure.[24−29] In this work, we show that this problem can be solved by adding a third material into the Au/oxide binary system, whose role is solely for stabilizing Au particles without interfering with the original high activity. The geometrical and electronic properties of such a ternary system are demonstrated, providing new insights into catalyst design.

Recent studies on oxide-supported Au catalysts have suggested that reducing oxide surfaces might help to stabilize Au particles.[30,31] It was reported that Au particles preferentially reside on surface oxygen vacancy sites for oxides such as TiO_2, MgO, and CeO_2.[30−34] However, it was also recognized that reducing the oxide support to prevent Au sintering is not a good strategy in general as many oxides (MgO, SiO_2, Al_2O_3, ZrO_2, et al.) are hardly reducible and that surface oxygen vacancies can be readily healed under ambient conditions.[35−37] Perhaps, a more practical method is to modify the geometric and electronic structure of the support by depositing or doping a second material onto the original oxide.[38,39] Aiming to find inexpensive, active, and stable materials designed for optimal performance, many different combinations of multiple-oxide supports have been tested in Au-based catalysts in the past few years, for example, Au/SiO_2-TiO_2, Au/TiO_2-ZrO_2, $Au/CeO_2-Al_2O_3$, and Au/MnO_2-CeO_2, but unfortunately, there are few successes.[39−47] In the case of $Au/IrO_2/TiO_2$ (rutile) catalyst for CO oxidation,[46,48] for example, the addition of IrO_2 was shown to greatly improve the stability of nanogold particles. Density functional theory (DFT) studies found that although IrO_2 with unsaturated d states can interact more strongly with Au than TiO_2, the activity of the ternary system is entirely due to the Au/IrO_2 boundary with the original activity of Au/TiO_2 being removed.[48] This is not desirable as the late transition metal oxide such as IrO_2 is not cost effective and is also more volatile than TiO_2.

More recently, Yan et al. synthesized alumina thin layer on TiO_2(anatase) (Al_2O_3/TiO_2) and the subsequent deposition of Au on the Al_2O_3/TiO_2 dual oxide produced a highly stable catalyst which remains to possess high activity for CO oxidation even after calcination at 773 K.[49] By utilizing high-resolution transmission electron microscopy (HRTEM), they showed that the size of Au particles increases markedly on TiO_2 but only slightly on Al_2O_3/TiO_2 at high temperatures.[49] As Al_2O_3 is insulating and inert toward reduction, the Al_2O_3 site in Al_2O_3/TiO_2 is expected to lack any of the known factors that could enhance Au sticking such as oxygen vacancies, metallic electrons, or unsaturated d states. It is thus very surprising that the combination of these two very common oxides can function

* Corresponding author. E-mail: zpliu@fudan.edu.cn.

10.1021/jp074530u CCC: $37.00
Published on Web 08/22/2007

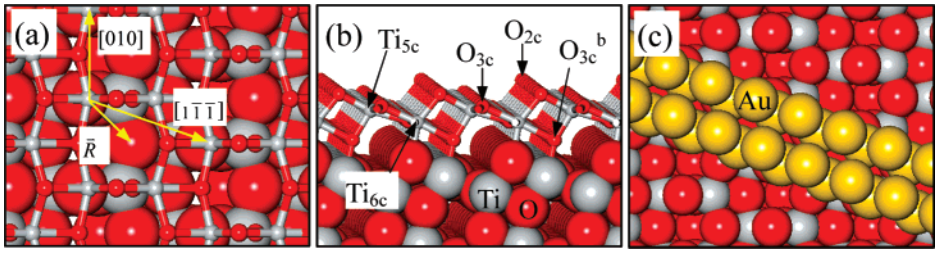

Figure 1. (a) Top and (b) side views of the structure of anatase TiO_2(101). (c) The optimized structure of the Au strip on anatase TiO_2(101).

as a better substrate for stabilizing Au particles. Moreover, as the Au/γ-Al_2O_3 system is a well-known poor catalyst for CO oxidation,[7,50] it is not clear why Au/Al_2O_3/TiO_2 can exhibit high catalytic ability, similar to Au/TiO_2.

With the aim to establish a general theoretical framework for designing proper support for Au/oxide catalysis, in this work, we carried out extensive first principles simulations to understand the physical origin of the synergetic effect in the Au, Al_2O_3, and TiO_2 ternary system. Since only rutile TiO_2 was thoroughly studied previously for Au/TiO_2 catalysis, the effect of the anatase phase in the system is of particular interest. To study the dual oxide, we have developed a systematic method to determine the structure of alumina on anatase, which takes into account both the kinetics and the thermodynamics in the alumina growth. The dual oxide is predicted to be a general-purpose support for stabilizing a group of catalytically important metals, including Au, Ag, Cu, Pt, Ir, and Pd, and thus, the results described here are of general interests in chemistry.

This paper is organized as follows. The calculation methods are described in section 2. In section 3, the catalytic activity of Au/TiO_2(anatase) for CO oxidation is first reported. Then, the structures for AlOOH and Al_2O_3 on anatase TiO_2 and the adsorption behavior of Au on the dual oxide are detailed, which is followed by the results on the origin of CO oxidation activity of the ternary system. Finally, general implications of the work are discussed in section 4, and the conclusions are summarized in section 5.

2. Computational Methods

All density functional theory calculations were performed using SIESTA package with numerical atomic orbital basis sets and Troullier−Martins norm-conserving pseudopotentials (scalar relativistic for heavy elements).[51−53] The semicore states (3s, 3p) for Ti had been treated explicitly. The exchange−correlation functional used was the generalized gradient approximation method, known as GGA-PBE.[54] A triple-ζ plus double-ζ polarization basis set (TZDP) was employed.[52,55] The orbital-confining cutoff radii were determined from an energy shift of 0.005 eV. The energy cutoff for the real space grid used to represent the density was set as 150 Ry. To further speed up calculations, the Kohn−Sham equation was solved by an iterative parallel diagonalization method that utilizes the ScaLAPACK subroutine pdsygvx with two-dimensional block cyclicly distributed matrix. The Broyden method was employed for geometry relaxation until the maximal force on each relaxed atom was less than 0.1 eV/Å. A constrained minimization scheme was employed to search the transition states (TSs) of the catalytic reactions.[56,57] The TS is identified when (i) the force on the atoms vanish and (ii) the energy is a maximum along the reaction coordinate but a minimum with respect to all of the other degrees of freedom.

Anatase TiO_2(101) was used to model the anatase substrate because it is the most stable and thus dominant surface in anatase TiO_2.[58] The (101) surface was modeled by a large unit cell [p(3 $\times$ 3), 16.65 Å $\times$ 11.40 Å] with the vacuum separation being more than 15 Å. Because of the large unit cell utilized and the insulating oxide support, only Γ point was used to sample the Brillouin zone in our calculations. The clean anatase TiO_2 surface modeled includes three layers [two TiO_2 units per layer in a p(1 $\times$ 1) cell] with the bottom layer fixed at the bulk-truncated structure. For AlOOH and Al_2O_3 deposited systems, two layers of TiO_2(101) were used as the substrate and the top layer were relaxed together with all Al-containing species. Other calculation details are as those described in the previous work,[21,59,60] where the accuracy of the SIESTA method was carefully benchmarked with a plane-wave methodology.

3. Results

3.1. CO Oxidation Over Au/TiO_2(Anatase). Before the catalytic activity of Au on the dual-oxide is investigated, CO oxidation on Au/TiO_2(anatase) has to be addressed. It is known that the Au/TiO_2 catalysis must involve both rutile and anatase phases of TiO_2 because of the high concentration of the anatase phase in small TiO_2 particles.[58] However, because of the difficulty in obtaining a large TiO_2 anatase crystal, previous studies mainly focused on rutile TiO_2, which is the most stable form of titania.[58] Experiments have shown that Au particles supported on rutile TiO_2(110) (the most stable surface of rutile) do exhibit high catalytic activity for CO oxidation, which has later been confirmed and rationalized by DFT calculations.[6,21] Here, we will see whether the anatase phase has any additional effect on activity.

The anatase TiO_2(101) surface consists of two-coordinated O (O_{2c}), three-coordinated O (O_{3c}), five-coordinated Ti, and six-coordinated Ti (see Figure 1). Considering that the presence of oxygen vacancies (reduced surface) might affect the catalytic activity considerably, we have investigated the possibility to create oxygen vacancies on the surface. We found that the energy required to remove any individual surface oxygen [in a p(3 $\times$ 3) cell] is over 4.0 eV with respect to 1/2 O_2 in the gas phase. This proves that anatase TiO_2 is hardly reducible under mild experimental conditions, and therefore only the defect-free anatase TiO_2(101) surface is employed hereafter to address its chemistry.

To model Au/TiO_2(anatase) system, we have added a two layer Au strip [24 atoms per p(3 $\times$ 3) supercell] on the top of the anatase TiO_2(101) surface, as shown in Figure 1c. The structure has been fully optimized by combining Nose thermostat molecular dynamics with Broyden minimization. This method of modeling has been successfully applied to study Au/TiO_2-(rutile) and a series of Au/ZrO_2 systems previously.[21,60] We found that the Au strip attaches to the TiO_2 surface mainly through the protruded bridging O_{2c}, forming six Au−O_{2c} bonds in the supercell (distance <2.5 Å). The adsorption energy of the Au strip hereafter is defined as E_{ad}(Au strip) = [E^{tot}(oxide) + E^{tot}(Au strip) − E^{tot}(Au/oxide)]/$N_{first\ Au}$, where E^{tot}(X) is the DFT total energy of the system X; for example, E^{tot}(Au strip) is the DFT total energy of the Au strip in the absence of the

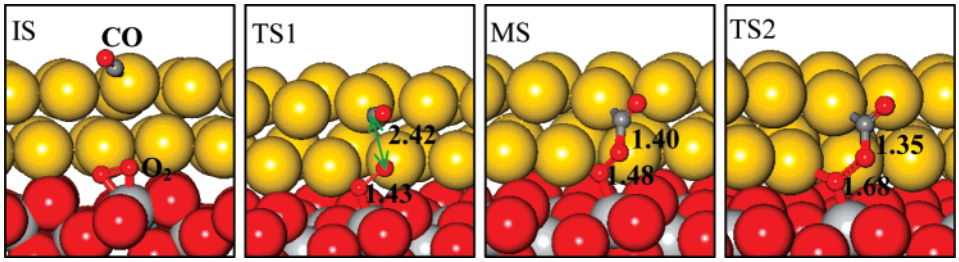

Figure 2. Calculated initial- (IS), transition- (TS1 and TS2), and meta-stable (MS) structures of CO oxidation over $Au/TiO_2(101)$. The distances (angstroms) of important bonds are also labeled.

support; $N_{\text{first Au}}$ is the number of the first-layer Au atoms that are in close contact with the oxide (i.e., Au−O distance shorter than 2.5 Å). The calculated E_{ad}(Au strip) for Au/TiO_2(anatase) is 0.15 eV per Au−O bond (there are six Au−O bonds per supercell). The weak adsorption of Au is quite typical for Au on defect-free oxide surfaces, such as rutile TiO_2 and ZrO_2 surfaces,[21,60] and is consistent with the fact that Au particles tend to agglomerate at elevated temperatures.

Analogous to that in Au/TiO_2(rutile),[21] CO oxidation is found to occur at the boundary between Au and TiO_2(anatase) by following a bimolecular pathway, namely, $CO + O_2 \rightarrow CO_2 + O$. Figure 2 shows the snapshots of the calculated initial, transition, and intermediate states for CO oxidation. We found that O_2 molecule adsorbs most strongly at the boundary of Au/TiO_2(anatase) with the adsorption energy of 1.30 eV, and CO can adsorb at the top site of the second Au layer with the adsorption energy of 0.65 eV in the presence of O_2. The adsorbed O_2 is spin-unpolarized with much lengthened O−O distance (1.44 Å). The adsorbed CO can then react with the adsorbed O_2 by overcoming a reaction barrier of 0.22 eV, which forms a transient OOCO compound. The OOCO intermediate (MS) is metastable and feasible to dissociate into a CO_2 and an adsorbed O atom, the barrier of which is only 0.06 eV.

Our calculations show that Au supported on anatase TiO_2 is also very active for CO oxidation even at low temperatures, which agrees well with the experimental observation.[6,49] We found, interestingly, that there is no obvious difference in the activity of CO oxidation between rutile and anatase phases since the calculated barriers are rather close, around 0.2 eV.[21] It should be emphasized that the adsorption of Au on both phases is rather weak, which suggests that the sintering of Au particles at high temperatures is inevitable. It is thus natural to ask why the addition of alumina can hinder the sintering process.

3.2. CO Oxidation Over Au Supported on Al_2O_3 Modified TiO_2. Experimentally, the alumina thin layer on TiO_2 was prepared by the surface sol−gel method, which utilized $Al(OR)_3$ (alkoxide, R = alkyl) as the precursor to react with surface OH groups of the oxide.[49] As the reaction is self-limiting, it allows controlling the interfacial thickness and composition with molecular precision by simply iterating $Al(OR)_3$ deposition and hydrolysis.[61] Because the thin layer was synthesized step-wisely, that is, kinetically controlled, it is expected that the theoretical method to determine structure has to take into account the kinetics. In this work, our theoretical simulation to characterize the structure of alumina modified TiO_2 is entirely guided by the formation energetics from first principles DFT calculations, and the simulation procedure mimics the way how the thin layer was prepared in the experiment.[49] Noticeably, this method is distinct from ab initio thermodynamics,[62] which was commonly utilized in recent years to determine the most stable surface structures at a particular temperature and pressure, such as TiO_x film on Mo(112).[63]

According to the experiment, the formation of various forms of alumina on TiO_2 can be generalized by the following formula:

$$n\text{Al(OH)}_3 + \text{TiO}_2 \rightarrow (\text{AlOOH})_n/\text{TiO}_2 + n\text{H}_2\text{O} \quad (1)$$

$$n\text{Al(OH)}_3 + (\text{AlOOH})_n/\text{TiO}_2 \rightarrow (\text{Al}_2\text{O}_3)_n/\text{TiO}_2 + 2n\text{H}_2\text{O} \quad (2)$$

The $(AlOOH)_n/TiO_2$ and $(Al_2O_3)_n/TiO_2$ are the AlOOH species and Al_2O_3 film modified TiO_2(anatase) surfaces, respectively. Here, aluminum hydroxide [$Al(OH)_3$] is used as a reference, which defines a common zero energy level to calculate the stability of various Al-containing moieties on TiO_2. This can be done by measuring the formation energies ΔE_f according to the eqs 1 and 2. The formation energies ΔE_f of the AlOOH species and Al_2O_3 film on TiO_2 are defined by formula 3 and formula 4, respectively, which is with respect to the gas-phase H_2O, $Al(OH)_3$, and a clear TiO_2 surface.

$$\Delta E_f(\text{AlOOH}) = \{E^{\text{tot}}[(\text{AlOOH})_n/\text{TiO}_2] + n \times E^{\text{tot}}[\text{H}_2\text{O}] - n \times E^{\text{tot}}[\text{Al(OH)}_3] - E^{\text{tot}}[\text{TiO}_2]\}/n \quad (3)$$

$$\Delta E_f(\text{Al}_2\text{O}_3) = \{E^{\text{tot}}[(\text{Al}_2\text{O}_3)_{n/2}/\text{TiO}_2] + 3n/2 \times E^{\text{tot}}[\text{H}_2\text{O}] - n \times E^{\text{tot}}[\text{Al(OH)}_3] - E^{\text{tot}}[\text{TiO}_2]\}/n \quad (4)$$

where n is the total number of Al atoms in the supercell, E^{tot}-(X) is the DFT total energy of the system X. As can be seen from the definition, ΔE_f is the energy gain associated with each Al moiety upon adsorption. It should be emphasized that the structures of AlOOHs are important as they are precursors for Al_2O_3/TiO_2 in this kinetically controlled growing process.

3.2.1. Structures of AlOOHs on Anatase TiO_2. There are two possible ways for an AlOOH to reside on TiO_2(101): (i) the Al at the bridge site between two edge O_{2c} (labeled as Al_b) and (ii) the Al on the top of an edge O_{2c} (labeled as Al_t). The Al_b geometry is obviously more favorable at low AlOOH coverages since more Al−O_{2c} bonds are formed. We have gradually built up AlOOH in the Al_b geometry up to 1/2 monolayer (ML). Our calculated ΔE_f for AlOOH on TiO_2(101) are −1.70, −1.67, −1.40, and −1.21 eV for 1/18, 1/6, 1/3, and 1/2 ML, respectively. Here, the coverage of Al is defined as the ratio of the number of Al to that of Ti. Some representative structures are illustrated in Figure 3. It can be seen that the Al atoms are coordinated with four O atoms in the tetrahedral configuration. The tetrahedral structure of Al was already observed for aluminum oxide film growth on NiAl(110).[64,65] The results also indicate that the well-separated AlOOH monomer is quite stable, but its stability drops sharply with the increase of coverage. The strong repulsive interaction between AlOOH may be understood when considering that Al atoms start to share bonding with the same surface O_{2c} atoms above 1/6 ML while

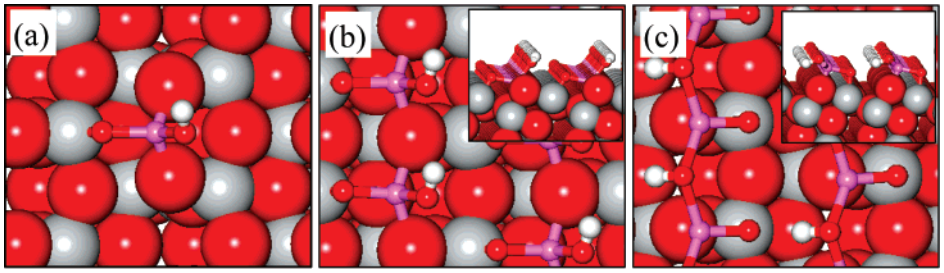

Figure 3. Structures of AlOOH on TiO_2(101). (a) 1/18 ML with an Al_b structure, (b) 1/2 ML with Al at the bridge site between two O_{2c}, and (c) 1/2 ML with Al at the top sites of O_{2c}. The insets are the side views.

the number of Al−O bonds per AlOOH keeps constant. This surface-mediated repulsive effect, known as bonding competition effect, has been well-addressed previously for adsorbates on metal surfaces.[66]

It should be mentioned that we also examined the AlOOH structure in the Al_t geometry at 1/2 ML, as represented in Figure 3c. In this structure, the formation energy of AlOOH is only −0.94 eV, which is indeed less than that of the Al_b counterpart (Figure 3b). By comparing the two structures, we may understand their relative stability as follows. The 1/2 ML AlOOH with Al_b geometry has one more Al−O_{2c} bond but one less Al−OH bond compared with the one with Al_t geometry. Since the Al−O bond is largely ionic, it can be deduced that the O_{2c} being more negatively charged can form a stronger bond with Al than with the OH group. Therefore, the Al_b structure is more stable than the Al_t structure at the coverage.

3.2.2. Structures of Al_2O_3 Films on Anatase TiO_2. Above 1/2 ML, dehydrated aluminum oxide starts to form by reacting newly arrived $Al(OR)_3$ (R = alkyl) with surface AlOOH. Since the intermediate coverages, that is, between 1/2 and 1 ML, contains both AlOOH and dehydrated Al_2O_3 and are very complex in structure, we have gone directly to investigate the fully dehydrated Al_2O_3 film at 1 ML, which may occur when the local coverage of Al is high. The formation energy of 1 ML film is important in thermodynamics as it dictates the growing mode (e.g., clustering or spreading) of alumina on anatase TiO_2. Among many possible structures for the full coverage of Al_2O_3 film investigated, we have obtained three stable Al_2O_3 films on TiO_2 (Al_2O_3/TiO_2). They are elaborated in the following paragraphs, and their structures are shown in Figure 4.

Film A: This is the most stable film structure with ΔE_f being −1.39 eV. All Al in the film are in the distorted-octahedral structure with five O coordinations. Each Al is directly above a surface O of TiO_2(101) and is interlinked by four-, three-, and two-coordinated O atoms. More specifically, the Al_2O_3 film can be considered as a surface layer of TiO_2(101) shifted along the direction that is 20.0° clockwise rotated from the $[1\bar{1}1]$ vector (see $\bar{R}$ in Figure 1), in which Ti cations are replaced by Al and all bottom O atoms of the layer ($O_{3c}{}^b$ as labeled in Figure 1) are removed. The Al_2O_3 film thus looks very similar to the TiO_2(101) surface, for example, also exposing two-coordinated bridging O. The nice match of the Al_2O_3 film to TiO_2(101) may not be too surprising as the Al−O bond distances in bulk α-Al_2O_3 (1.86 and 1.97 Å) are very close to the Ti−O distances in anatase TiO_2 (1.93 and 1.97 Å).

It should be emphasized that the distorted-octahedral structure of Al is distinct from that of bulky alumina and has not been reported before. From Figures 3 and 4, we can also see that film A can be directly built up from the 1/2 ML Al_t structure (Figure 3c) by populating another 1/2 ML AlOOH in between the O_{2c}. This is interesting as the 1/2 ML Al_t structure is not the most stable one for alumina at 1/2 ML, indicating the reconstruction of the Al structure occurs with the increase of Al coverage.

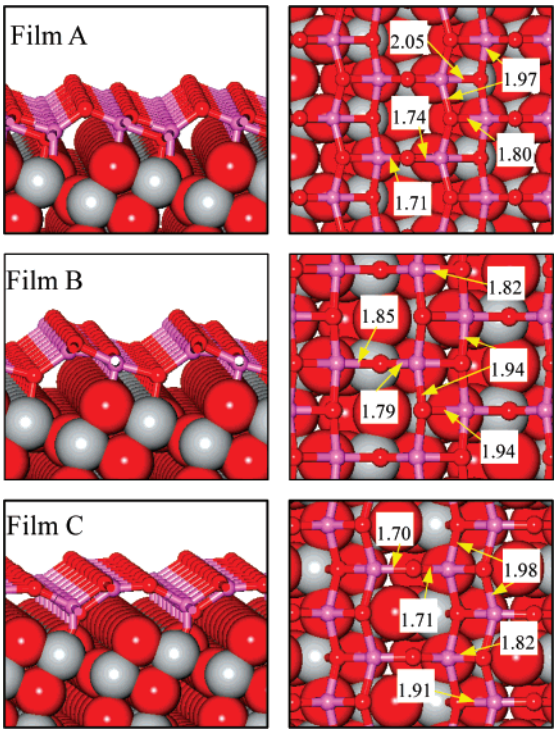

Figure 4. Three different structures of 1 ML Al_2O_3 films on TiO_2-(101). Left column, side view; right column, top view. The distances (angstroms) of selected Al−O bonds are labeled.

Film B: This is the less stable film with ΔE_f being −1.28 eV. The structure of the film is identical to that of a surface layer of TiO_2(101) except the edge O_{2c} is absent. In this structure, Al atoms are evenly divided into two types: four- and five-coordinated, while all of the surface O atoms are three-coordinated. Film B is also derived from the 1/2 ML Al_t structure with each additional Al linking with only one O_{2c}.

Film C: The structure is the least stable one with ΔE_f being −1.14 eV. In this structure, half of the Al atoms are four-coordinated and the others are five-coordinated. The film was borne out from Nose molecular dynamic simulation at 300 K, which induces significant local structural relaxation on our initially guessed geometry. The precursor of the film can be considered as a surface layer of TiO_2(101) shifted along the (010) direction by a half lattice unit, in which Ti are replaced by Al and all $O_{3c}{}^b$ are removed.

Further increasing the coverage, we found that multiple Al_2O_3 layers can grow on top of the most stable film A in an epitaxial mode. Al_2O_3 films up to 4 ML have been investigated. As a representative, the structure of 3 ML Al_2O_3 on TiO_2(101) is illustrated in Figure 5. The calculated stability of Al_2O_3 on TiO_2-

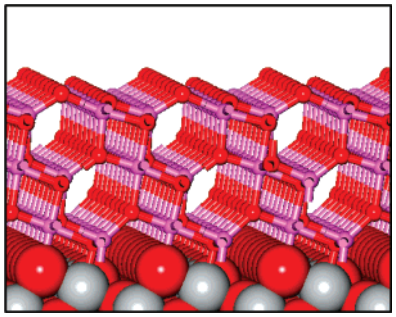

Figure 5. Structure of 3 ML Al_2O_3 film on TiO_2(101).

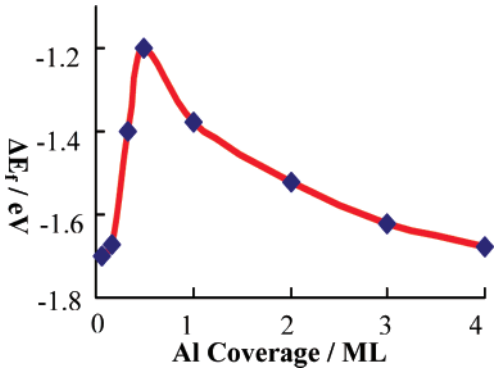

Figure 6. Plot of the formation energies of AlOOH and Al_2O_3 on TiO_2(101) versus Al coverage.

TABLE 1: Formation Energies ΔE_f, the Band Gap ΔE_{gap}, and the Au Atom Adsorption Energy E_{ad}(Au) for Al_2O_3 Fully Covered TiO_2(101) at Different Al Coverages[a]

	TiO_2(101)	1 ML	2 ML	3 ML	4 ML
ΔE_f		−1.39	−1.52	−1.62	−1.68
ΔE_{gap}	1.98	0.75	0.13	<0.1	<0.1
E_{ad}(Au)	0.43	2.07	3.00	3.78[b]	4.13[b]

[a] The data for clean TiO_2(101) is also listed for comparison. The unit of energy is electronvolts. [b] The results were calculated using double-ζ plus polarization (DZP) basis set.

(101) increases as the film grows (see Table 1). We also noticed that, as the layer of Al_2O_3 film increases, the band gap of the Al_2O_3/TiO_2 system decreases, from 0.75 eV at 1 ML to nearly 0 eV above 3 ML. This indicates that the thickness of the deposited Al_2O_3 film can strongly affect the electronic structure of the system.

Overall, the formation energies versus Al coverage for AlOOH and Al_2O_3 growth on TiO_2(101) can be summarized in Figure 6. As addressed, the stability of AlOOH is very sensitive to the Al coverage due to the strong repulsive interaction. Above 1/2 ML coverage, dehydrated Al_2O_3 starts to form, which recovers the stability of Al-containing species gradually. Eventually, multiple layers of Al_2O_3 can be as stable as the well-separated AlOOH monomer. The results demonstrate that Al-containing species on anatase TiO_2 should either be finely dispersed at low coverages or be clustering into thick Al_2O_3 islands at relative high coverages. In other words, a very thin layer of Al_2O_3 on anatase TiO_2 is not favored on the basis of thermodynamics. This implies, on the other hand, that the kinetically controlled process utilized in experiment[49] is absolutely essential in obtaining Al_2O_3 thin layers. Even with such a procedure, we would expect the prepared alumina layers are not uniform in thickness, and thus the exposed TiO_2 sites are available.

3.2.3. Adsorption of Au on Al_2O_3/TiO_2. Using Au atom as the probe, we examined the adsorption behavior of atomic Au

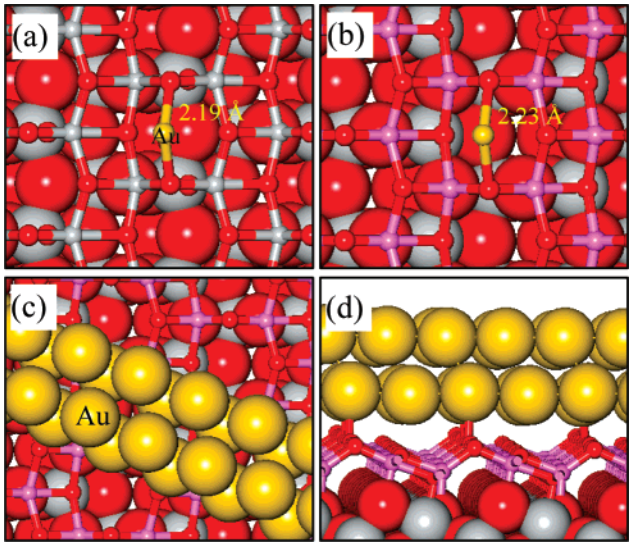

Figure 7. Optimized structures of Au atom on (a) TiO_2(101) and (b) Al_2O_3 (1 ML)/TiO_2, and a two-layer Au strip on Al_2O_3 (1 ML)/TiO_2 (c, top view; d, side view). The distances of Au−O bonds are also labeled.

TABLE 2: Adsorption Energies (Electronvolts) of Various Metal Atoms on TiO_2(101) and Al_2O_3 (1 ML)/TiO_2

	Ag	Cu	Pt	Pd	Ir
TiO_2(101)	1.04	2.19	3.27	1.43	3.28
Al_2O_3/TiO_2	2.80	3.93	3.57	2.56	4.86

on the determined Al_2O_3/TiO_2 surface, which was compared to it on a clean TiO_2(101) surface. Among several possible configurations for its adsorption, we found that the most favorable adsorption site is the bridge site between two neighboring O_{2c} atoms on both TiO_2 and Al_2O_3/TiO_2 (see Figure 7). It can be seen that the adsorption of Au atoms on TiO_2 is increased to the value of 2.07 eV by the deposition of Al_2O_3 film, which is about five times higher than that on TiO_2(101) (see Table 1). Moreover, with the increase of the Al_2O_3 film thickness, the adsorption energy of the Au atom also increases. The calculated adsorption energies are 3.00, 3.78, and 4.13 eV for Au on the 2−4 layer Al_2O_3 films on TiO_2, respectively. These values are remarkable if we consider that the cohesive energy of bulk Au is ∼3.20 eV and the adsorption energy of the Au atom on α-Al_2O_3(001) surface is about 0.75 eV from our DFT calculations and previous theoretical results.[67,68]

On going from an atom to the Au strip, we found the similar phenomenon. We modeled the $Au/Al_2O_3/TiO_2$ system by adding a two layer Au strip on the Al_2O_3/TiO_2 (see Figure 7), similar to what we have done for Au on anatase TiO_2(101). The calculated adsorption energies of the Au strip on the 1 and 2 ML Al_2O_3 films covered TiO_2(101) are 0.78 and 1.54 eV per Au−O_{2c} bond (there are six Au−O_{2c} bonds in the supercell), respectively (as compared with 0.15 eV for the Au strip on clean TiO_2 surface). The strong interaction between Au and the Al_2O_3 overlayer supports the observed ultrastability of Au on the Al_2O_3 modified anatase TiO_2.[49]

It is also interesting to examine whether the Al_2O_3/TiO_2 surface can enhance the adsorption of other metals. Table 2 lists our calculated adsorption energies of Ag, Cu, Pt, Pd, and Ir atoms on TiO_2(101) and the 1 ML Al_2O_3 film covered TiO_2-(101) [Al_2O_3 (1 ML)/TiO_2]. As shown in Table 2, the adsorption energies of all of these metals are improved in the presence of the Al_2O_3 film. This indicates that the controlled growth of alumina on anatase TiO_2 could be a general way to improve the stability of metal particles.

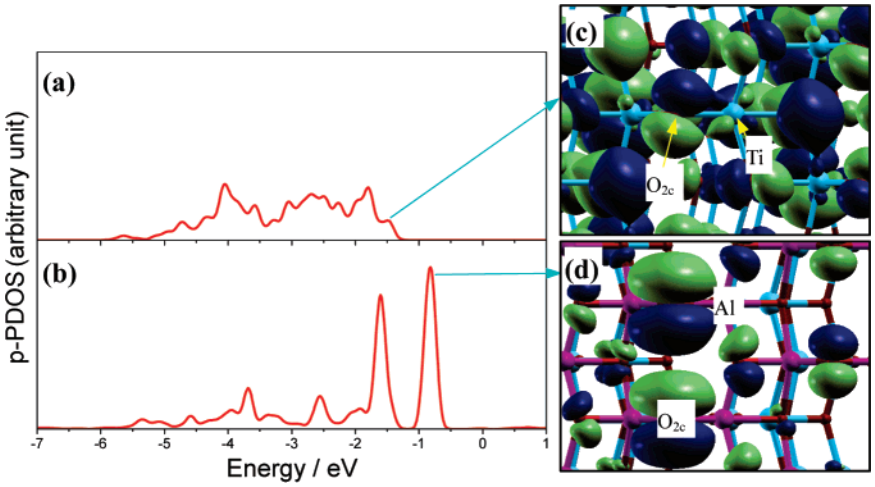

Figure 8. DOS projected onto 2p orbitals of O_{2c} atoms in (a) $TiO_2(101)$ and (b) Al_2O_3 (1 ML)/TiO_2 and the selected Kohn−Sham orbitals with isosurface value at ± 0.01 au for (c) $TiO_2(101)$ and (d) Al_2O_3 (1 ML)/TiO_2. The curves are aligned by matching a semicore Ti state in the bottom layer of the slab.

To reveal the physical origin of the strong bonding between Au and Al_2O_3/TiO_2, we have investigated the electronic structure of the systems in detail. First, we calculated the density of states (DOS) of $TiO_2(101)$ and the Al_2O_3 (1 ML)/TiO_2 projected onto the 2p orbitals of surface O_{2c}, which are plotted in Figure 8. We found that the p-projected DOS of O_{2c} differs significantly between the two systems. In the Al_2O_3/TiO_2, a significant portion of p states locates near the Fermi level, which is in the range of −1.5 to 0 eV. This portion of p states is mainly nonbonding 2p states, which can be seen from the contour plot of the corresponding Kohn−Sham orbital (see Figure 8). By contrast, in TiO_2, the O_{2c} p states spread over a wide energy window from −5.0 to −1.5 eV because of their strong interaction with Ti d states. The p−d orbital mixing can be clearly viewed from the Kohn−Sham orbital contour plot in Figure 8c. We found that although both O_{2c} are apparently two-coordinated, the p−d orbital mixing that is not present for O_{2c} in the Al_2O_3/TiO_2 is the key driving force to stabilize the p orbitals of O_{2c} in $TiO_2(101)$. It is thus expected that the O_{2c} atoms in the Al_2O_3/TiO_2 with high-energy p electrons should be more active than the O_{2c} atoms in $TiO_2(101)$.

Next, we examined the bonding nature of Au on the surfaces by plotting the difference of the density of states (Δp-PDOS) projected onto 2p orbitals of O_{2c} atoms in $TiO_2(101)$ and the Al_2O_3 (1 ML)/TiO_2 before and after the Au atom adsorption (see Figure 9). In the Δp-PDOS, the energy region with negative values usually belongs to those O_{2p} states that are strongly involved in chemically bonding with Au atom and thus split into bonding and antibonding states which appear elsewhere. As shown, the nonbonding state of O_{2c} in Al_2O_3/TiO_2 interacts strongly with the Au valence orbital, leading to the increase of DOS at much lower energy regions. By contrast, the O_{2c} in TiO_2 is less perturbed by Au. The energy gain from the Au−O_{2c} bond formation (−6.0 ∼ −4.0 eV) is largely cancelled by the energy cost due to the filled antibonding states at −1.5 ∼ 0 eV. In short, the high stability of Au on Al_2O_3/TiO_2 can be attributed to the availability of the highly active O_{2c} in the Al_2O_3 film, which can form strong covalent bonds with Au.

3.2.4. CO Oxidation Activity of the Ternary System. For CO oxidation over supported Au catalysts, it is known that the adsorption and activation of the O_2 molecule is the key step.[21] Previous studies have shown that O_2 adsorbs very weakly (below 0.2 eV) on pure Au surfaces and the Au/MgO system.[22,56] As a result, CO oxidation on the systems has to follow the Eley−

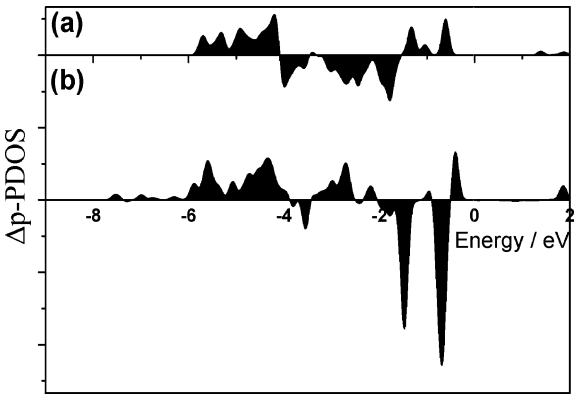

Figure 9. Plots of the difference of DOS projected onto 2p orbitals of O_{2c} atoms (Δp-PDOS) in (a) $TiO_2(101)$ and (b) Al_2O_3 (1 ML)/TiO_2 due to the Au atom adsorption. The curves are aligned by matching a semicore Ti state in the bottom layer of the slab.

Rideal mechanism,[69] which is believed to be the main reason for their low activity in CO oxidation. On the other hand, as we already revealed in the Au/TiO_2 system, O_2 can adsorb strongly at the Au/TiO_2 boundary, and CO oxidation occurs much more efficiently in the Langmuir−Hinshelwood mechanism.[21]

We have explored all of the possible configurations for the O_2 adsorption at Au/Al_2O_3 (1 ML)/TiO_2, including the boundary between Au and Al_2O_3/TiO_2. We can indeed identify an adsorption state for O_2 at the boundary of the Au strip and the Al_2O_3/TiO_2, where one end of O_2 bonds with a surface Al cation and the other end bonds with the first layer Au atoms. Despite that this adsorption structure resembles what we found for O_2 at the Au/TiO_2, the corresponding adsorption energy of O_2 is poor, only 0.10 eV, which means that O_2 does not adsorb at ambient conditions (at finite temperatures the entropy contribution to Gibbs free energy of the gas-phase O_2 can easily exceed 0.10 eV). Consistently, this O_2 molecule remains to be spin polarized (0.38 μ_B). Furthermore, we repeated our calculations for O_2 adsorption at Au/Al_2O_3 (2 ML)/TiO_2. Similarly, O_2 adsorption at the Au/dual-oxide boundary, where one end of O_2 bonds with an Al cation and the other end bonds with the first layer Au, is found to be energetically infeasible; that is, O_2 at the boundary between Au and Al_2O_3 (2 ML)/TiO_2 is even less stable than it is in the gas phase.

In fact, the low adsorption of O_2 on top of Al sites may not be surprising. It is known that Au supported on γ-Al_2O_3

performs poorly for CO oxidation.[50] The poor activity of Au/Al_2O_3 falls in the same category together with some other systems, such as Au/MgO and Au/SiO_2.[70] Our recent work for CO oxidation over the Au/ZrO_2 system has shown that the empty d states of cations are essential for O_2 adsorption and activation, which can strongly mix with the O_2 $2\pi^*$ orbitals.[60] The missing of d states in the oxide cations would cause the low O_2 adsorption/activation, which explains the poor activity of the systems like Au/MgO. This understanding can be well-extended to rationalize our finding for O_2 at Au/Al_2O_3/TiO_2.

Obviously, without O_2 adsorption, CO oxidation at Au/Al_2O_3/TiO_2(anatase) cannot follow the Langmuir−Hinshelwood mechanism, and thus it is expected that the Au/Al_2O_3/TiO_2 alone is not a good catalyst for CO oxidation. In other words, once TiO_2 is fully covered by alumina, CO oxidation activity would also diminish. Nevertheless, from the energetics of alumina growth on TiO_2, we already pointed out that alumina on TiO_2 is not uniform in structure and the exposed TiO_2 sites should be present, which could then contribute to CO oxidation when contacting with Au. In this architecture, alumina in the ternary system acts only as the anchoring center for Au particles, while the boundary of Au and TiO_2 provides the active site for CO oxidation. We also noticed that the onset temperatures of CO oxidation are similar (~230 K) with or without alumina as found by Yan et al.[49] This evidence supports our conclusion that alumina itself does not take part in CO oxidation.

4. General Discussions

From our results, the alumina thin layer on TiO_2 does significantly affect the thermal stability of the catalyst but has no contribution to the activity. The physical origin of these is all related to the lack of d states in alumina. First, the two-coordinated O exposed in the alumina layer is very active due to the lack of p−d orbital mixing, which leads to the high adsorption of Au on alumina/anatase. Second, the surface without d states is a poor substrate in activating O_2. The electronic structure of the ternary system determines that only the boundary of Au/TiO_2 can be active for CO oxidation, while the alumina is not a catalytically active component.

The enhanced Au stability relies on the unique structure of the alumina layer, which in turn is pinned by the underneath anatase TiO_2 surface. It is therefore worth mentioning the important role of the anatase phase. In fact, we have also tentatively constructed the alumina film on the rutile TiO_2(110) surface but failed to obtain any reasonable structures. We found that the anatase TiO_2(101) surface has an important feature, namely, the presence of $O_{3c}{}^b$ (see Figure 1) in the first layer. The $O_{3c}{}^b$ bridge the two types of top layer Ti cations and act as a linkage between the first and the second layer. In constructing the structure of the alumina film using TiO_2 surface as the template, it is inevitable to get rid of excess O because of Al being less formally charged than Ti. By deleting $O_{3c}{}^b$, we can see that only one coordination is lost for each type of cations without destroying the connecting network of the first layer. Further, shifting the whole overlayer, we can readily obtain the film A structure, where the Al coordination is at least five, close to its bulk coordination number (six). By contrast, on rutile (110), the O linkage between the first layer and the second layer binds exclusively with the same type of cation (Ti) of the top layer. By removing these O, four coordinated cations are created, which, however, cannot be diminished by shifting the overlayer structure. Such an oxide surface structure with exposed low-coordinated cations is not stable, as already shown in the literature[71] and also our work (Film A is more stable than film B and C).

5. Conclusions

To recap, we have identified the working mechanism of a complex catalytic system from first principles calculations, that is, Au supported on alumina modified anatase TiO_2. Our results are as follows:

(i) For Au supported on pure anatase, CO oxidation is facile with the reaction barrier being 0.22 eV. Similar to Au on rutile TiO_2, Au binds only weakly with anatase.

(ii) A stepwise simulation procedure based on DFT was proposed and utilized to reveal the structure of alumina on anatase, which takes into account both kinetics and thermodynamics of the growth process. From the calculated formation energies for AlOOH and Al_2O_3 on anatase at different coverages, the alumina on anatase is found to be inhomogeneous with a strong tendency toward clustering. An unprecedented Al_2O_3 film structure on TiO_2 was characterized, which features two-coordinated O anions and Al cations in distorted-octahedral coordination geometry. This film structure corresponds to locally clustered Al_2O_3 domains.

(iii) The local Al_2O_3 film acts as the nucleation center to anchor Au particles, which can improve the Au binding energy on anatase by more than four times. Owing to the lack of d states in Al, the exposed two-coordinated O in the Al_2O_3 film possess nonbonding 2p states and thus can form strong covalent bonds with Au and a series of other metals.

(iv) The reaction site of this ternary system is still the Au/anatase boundary since Au on the alumina fully covered anatase would not be capable of adsorbing O_2. The alumina is thus not a catalytically active component.

The theory established here demonstrates how the synergetic effect among three components, that is, Au, alumina, and anatase, can influence profoundly both the geometrical and the electronic structures of the system. It shows that depositing one p-block oxide onto a d-block oxide could produce a material with entirely new electronic properties. This may help to clear up puzzles around catalyst activities of multiple-component catalysts and guide the development of catalysts using nonuniform mixed-oxide as support.

Acknowledgment. This work is supported by NSF of China (20573023, 20433020, 20673024), Pujiang Plan, and NSF of Shanghai Sci. Tech. Committee (06PJ14011, 05DZ22313). Shanghai Supercomputing Center is thanked for computing time. Z Ma is thanked for helpful discussions.

References and Notes

(1) Bartholomew, C. H. *Appl. Catal. A* **2001**, *212*, *17*.
(2) Campbell, C. T.; Parker, S. C.; Starr, D. E. *Science* **2002**, *298*, 811.
(3) Spencer, M. S.; Twigg, M. V. *Annu. Rev. Mater. Res.* **2005**, *35*, 427.
(4) Dixon, R. A.; Egdell, R. G. *J. Chem. Soc., Faraday Trans.* **1998**, *94*, 1329.
(5) Stone, P.; Poulston, S.; Bennett, R. A.; Bowker, M. *Chem. Commun.* **1998**, 1369.
(6) Haruta, M. *Catal. Today* **1997**, *36*, 153.
(7) Bond, G. C.; Thompson, D. T. *Catal. Rev. Sci. Eng.* **1999**, *41*, 319.
(8) Grisel, R.; Weststrate, K. J.; Gluhoi, A.; Nieuwenhuys, B. E. *Gold Bull.* **2002**, *35*, 39.
(9) Thompson, D. T. *Appl. Catal. A* **2003**, *243*, 201.
(10) Chen, M. S.; Goodman, D. W. *Acc. Chem. Res.* **2006**, *39*, 739.
(11) Arenz, M.; Landman, U.; Heiz, U. *ChemPhysChem* **2006**, *7*, 1871.
(12) Hashmi, A. S. K.; Hutchings, G. J. *Angew. Chem., Int. Ed.* **2006**, *45*, 7896.
(13) Valden, M.; Lai, X.; Goodman, D. W. *Science* **1998**, *281*, 1647.
(14) Comotti, M.; Li, W. C.; Spliethoff, B.; Schuth, F. *J. Am. Chem. Soc.* **2006**, *128*, 917.
(15) Stiehl, J. D.; Kim, T. S.; McClure, S. M.; Mullins, C. B. *J. Am. Chem. Soc.* **2004**, *126*, 13574.

(16) Yoon, B.; Hakkinen, H.; Landman, U.; Worz, A. S.; Antonietti, J. M.; Abbet, S.; Judai, K.; Heiz, U. *Science* **2005**, *307*, 403.
(17) Deng, W. L.; Flytzani-Stephanopoulos, M. *Angew. Chem., Int. Ed.* **2006**, *45*, 2285.
(18) Azar, M.; Caps, V.; Morfin, F.; Rousset, J. L.; Piednoir, A.; Bertolini, J. C.; Piccolo, L. *J. Catal.* **2006**, *239*, 307.
(19) Kim, C. H.; Thompson, L. T. *J. Catal.* **2005**, *230*, 66.
(20) Konova, P.; Naydenov, A.; Tabakova, T.; Mehandjiev, D. *Catal. Commun.* **2004**, *5*, 537.
(21) Liu, Z. P.; Gong, X. Q.; Kohanoff, J.; Sanchez, C.; Hu, P. *Phys. Rev. Lett.* **2003**, *91*, 266102.
(22) Molina, L. M.; Hammer, B. *Phys. Rev. Lett.* **2003**, *90*, 206102.
(23) Molina, L. M.; Rasmussen, M. D.; Hammer, B. *J. Chem. Phys.* **2004**, *120*, 7673.
(24) Moreau, F.; Bond, G. C. *Catal. Today* **2006**, *114*, 362.
(25) Zhu, H. G.; Liang, C. D.; Yan, W. F.; Overbury, S. H.; Dai, S. *J. Phys. Chem. B* **2006**, *110*, 10842.
(26) Andreescu, D.; Sau, T. K.; Goia, D. V. *J. Colloid Interface Sci.* **2006**, *298*, 742.
(27) Yan, W. F.; Brown, S.; Pan, Z. W.; Mahurin, S. M.; Overbury, S. H.; Dai, S. *Angew. Chem., Int. Ed.* **2006**, *45*, 3614.
(28) Schubert, M. M.; Plzak, V.; Garche, J.; Behm, R. J. *Catal. Lett.* **2001**, *76*, 143.
(29) Ivanova, S.; Petit, C.; Pitchon, V. *Gold Bull.* **2006**, *39*, 3.
(30) Sanchez, A.; Abbet, S.; Heiz, U.; Schneider, W. D.; Hakkinen, H.; Barnett, R. N.; Landman, U. *J. Phys. Chem. A* **1999**, *103*, 9573.
(31) Biener, J.; Biener, M. M.; Nowitzki, T.; Hamza, A. V.; Friend, C. M.; Zielasek, V.; Baumer, M. *ChemPhysChem* **2006**, *7*, 1906.
(32) Vittadini, A.; Selloni, A. *J. Chem. Phys.* **2002**, *117*, 353.
(33) Wallace, W. T.; Min, B. K.; Goodman, D. W. *J. Mol. Catal. A* **2005**, *228*, 3.
(34) Liu, Z. P.; Jenkins, S. J.; King, D. A. *Phys. Rev. Lett.* **2005**, *94*, 196102.
(35) Bikondoa, O.; Pang, C. L.; Ithnin, R.; Muryn, C. A.; Onishi, H.; Thornton, G. *Nat. Mater.* **2006**, *5*, 189.
(36) Wendt, S.; Matthiesen, J.; Schaub, R.; Vestergaard, E. K.; Laegsgaard, E.; Besenbacher, F.; Hammer, B. *Phys. Rev. Lett.* **2006**, *96*.
(37) Wendt, S.; Schaub, R.; Matthiesen, J.; Vestergaard, E. K.; Wahlstrom, E.; Rasmussen, M. D.; Thostrup, P.; Molina, L. M.; Laegsgaard, E.; Stensgaard, I.; Hammer, B.; Besenbacher, F. *Surf. Sci.* **2005**, *598*, 226.
(38) Wang, S. W.; Borisevich, A. Y.; Rashkeev, S. N.; Glazoff, M. V.; Sohlberg, K.; Pennycook, S. J.; Pantelides, S. T. *Nat. Mater.* **2004**, *3*, 143.
(39) Min, B. K.; Wallace, W. T.; Goodman, D. W. *J. Phys. Chem. B* **2004**, *108*, 14609.
(40) Yan, W. F.; Mahurin, S. M.; Overbury, S. H.; Dai, S. *Top. Catal.* **2006**, *39*, 199.
(41) Yan, W. F.; Mahurin, S. M.; Chen, B.; Overbury, S. H.; Dai, S. *J. Phys. Chem. B* **2005**, *109*, 15489.
(42) Lai, S. Y.; Zhang, H. X.; Ng, C. F. *Catal. Lett.* **2004**, *92*, 107.
(43) Chang, L. H.; Sasirekha, N.; Chen, Y. W.; Wang, W. J. *Ind. Eng. Chem. Res.* **2006**, *45*, 4927.
(44) Centeno, M. A.; Hadjiivanov, K.; Venkov, T.; Klimev, H.; Odriozola, J. A. *J. Mol. Catal. A* **2006**, *252*, 142.
(45) Zhang, F. L.; Zheng, Q.; Wei, K. M.; Lin, X. Y.; Zhang, H. H.; Li, J. W.; Cao, Y. N. *Catal. Lett.* **2006**, *108*, 131.
(46) Okumura, M.; Akita, T.; Haruta, M.; Wang, X.; Kajikawa, O.; Okada, O. *Appl. Catal. B* **2003**, *41*, 43.
(47) Grisel, R. J. H.; Nieuwenhuys, B. E. *J. Catal.* **2001**, *199*, 48.
(48) Liu, Z. P.; Jenkins, S. J.; King, D. A. *Phys. Rev. Lett.* **2004**, *93*, 156102.
(49) Yan, W. F.; Mahurin, S. M.; Pan, Z. W.; Overbury, S. H.; Dai, S. *J. Am. Chem. Soc.* **2005**, *127*, 10480.
(50) Arrii, S.; Morfin, F.; Renouprez, A. J.; Rousset, J. L. *J. Am. Chem. Soc.* **2004**, *126*, 1199.
(51) Soler, J. M.; Artacho, E.; Gale, J. D.; Garcia, A.; Junquera, J.; Ordejon, P.; Sanchez-Portal, D. *J. Phys.: Condens. Matter* **2002**, *14*, 2745.
(52) Junquera, J.; Paz, O.; Sanchez-Portal, D.; Artacho, E. *Phys. Rev. B* **2001**, *64*, 235111.
(53) Troullier, N.; Martins, J. L. *Phys. Rev. B* **1991**, *43*, 1993.
(54) Perdew, J. P.; Burke, K.; Ernzerhof, M. *Phys. Rev. Lett.* **1996**, *77*, 3865.
(55) Anglada, E.; Soler, J. M.; Junquera, J.; Artacho, E. *Phys. Rev. B* **2002**, *66*.
(56) Liu, Z. P.; Hu, P.; Alavi, A. *J. Am. Chem. Soc.* **2002**, *124*, 14770.
(57) Liu, Z. P.; Jenkins, S. J.; King, D. A. *J. Am. Chem. Soc.* **2004**, *126*, 10746.
(58) Diebold, U. *Surf. Sci. Rep.* **2003**, *48*, 53.
(59) Liu, Z. P.; Wang, C. M.; Fan, K. N. *Angew. Chem., Int. Ed.* **2006**, *45*, 6865.
(60) Wang, C. M.; Fan, K. N.; Liu, Z. P. *J. Am. Chem. Soc.* **2007**, *129*, 2642.
(61) Ichinose, I.; Senzu, H.; Kunitake, T. *Chem. Mater.* **1997**, *9*, 1296.
(62) Reuter, K.; Scheffler, M. *Phys. Rev. B* **2002**, *65*, 035406.
(63) Liu, Z. P. *Phys. Rev. B* **2006**, *73*, 233410.
(64) Kresse, G.; Schmid, M.; Napetschnig, E.; Shishkin, M.; Kohler, L.; Varga, P. *Science* **2005**, *308*, 1440.
(65) Stierle, A.; Renner, F.; Streitel, R.; Dosch, H.; Drube, W.; Cowie, B. C. *Science* **2004**, *303*, 1652.
(66) Liu, Z. P.; Hu, P. *J. Am. Chem. Soc.* **2003**, *125*, 1958.
(67) Wang, C. M.; Fan, K. N.; Liu, Z. P., unpublished results.
(68) Fernandez, E. M.; Balbas, L. C. *J. Phys. Chem. B* **2006**, *110*, 10449.
(69) Ertl, G. *Surf. Sci.* **1994**, *300*, 742.
(70) Yang, C. M.; Kalwei, M.; Schuth, F.; Chao, K. J. *Appl. Catal. A* **2003**, *254*, 289.
(71) Gong, X. Q.; Selloni, A.; Batzill, M.; Diebold, U. *Nat. Mater.* **2006**, *5*, 665.